A novel method to fully suppress single and bi-modal excitations due to the support vibration by means of piezoelectric actuators

Fabio Botta[a*], Andrea Rossi[a], Nicola Pio Belfiore[a]

Department of Engineering
University of Roma Tre
Via Vito Volterra, 62 - Rome, Italy

Abstract

Vibration attenuation and control is a typical topic in mechanical, civil and aeronautical engineering. In recent years, there has been extensive research on smart materials and among all of them, the piezoelectrics seem to be the most attractive for passive and active vibration damping applications. Furthermore if multiple modes are concurrently excited, as in case of turbomachinery blades, active damping systems may remarkably increase their life-cycle and outweigh the shortcomings of implementing such systems. However the damping efficiency of the piezoelectric actuators is strictly bound to their driving voltage, size and location on the structure.

In this work a cantilever piezoelectric bimorph beam under base motion is considered and the analytical expression of the electric potential that nullifies the elastic tip displacement of the beam is derived in case of single and bi-modal excitations.

The model allows to identify for every bi-modal excitations a set of solutions, each of them represented by three parameters: voltage amplitude, left and right corner positions of the piezoelectric actuators pair. As a result, designers can choose the best solution for their specific application demands. For example, if the supply voltage must to be kept as low as possible, then wider actuators

*Corresponding author
Email address: fabio.botta@uniroma3.it (Fabio Botta[a])

should be used and vice versa. It was also found out that the control parameters do not depend on the spectral distribution between the two excited modes. Hence, even if the spectral distribution between the two coupled modes changes over time, it is not necessary to adjust either the voltage or the position of the actuator pair.

The analytical predictions were compared with the results of FEM multi-physics simulations for several base motion excitations and a fair agreement was observed.

Keywords: Active vibration damping, piezoelectric, optimal placement

Nomenclature	
A	reference amplitude
$\mathbf{B}$	control vector
$\mathbf{C}$	damping matrices
d_{31}	piezoelectric coefficient
E_{a}	Young's modulus of the piezoelectric material
E_{b}	Young's modulus of the beam
I_{b}	moment of inertia of the beam
$\mathbf{K}$	stiffness matrices
L_{b}	beam length
M_{a}	piezoelectric bending moment
$\mathbf{M}$	mass matrices
r	ratio of the j-th component of the voltage
S	section area of the beam
t_{a}	piezoelectric thickness
t_{b}	beam thickness
V	voltage applied to the piezoelectric plates
γ	gain of the amplifiers
w	vertical displacement
w^{e}	vertical flexural displacement
w^{r}	vertical rigid motion
$\widetilde{w}$	virtual vertical displacement
α, β	damping coefficients
δL_{e}	virtual work of elastic forces
δL_{in}	inertial work of inertial forces
δL_{p}	virtual work of piezoelectric forces
ξ_1	dimensionless coordinate of the left edge of the piezoelectric actuator
ξ_2	dimensionless coordinate of the right edge of the piezoelectric actuator
ρ	mass density of the beam
$\phi_i(x)$	i-th flexural mode of the cantilever beam
ω_i	i-th natural frequency

1. Introduction

Vibration-related problems are widely addressed in many engineering fields because the structural vibrations may weaken the mechanical components and, in the worst cases, lead to fatigue failures. As a consequence, in the recent decades many strategies for vibration attenuation and control have been developed.

The availability of smart materials such as piezoelectrics, Shape Memory Alloys (SMA), Electro-Rheological (ER) and Magneto-Rheological (MR) fluids has provided new perspectives for vibration damping. In fact, a large number of works reported the implementation of novel smart-structures for vibrations and noise control, based on SMA [1–3], ER and MR fluids [4–9] and piezoelectric materials [10–14]. Among all the smart materials, the piezoelectric ones are the most employed for vibration applications because they ensure wide bandwidth, fast dynamic response and high resolution. Furthermore, when an electric potential is applied between their electrodes a deformation occurs and vice-versa, so this peculiar behavior make them suitable to be used both as sensors and actuators. Recently, piezoelectric materials have been increasingly embedded in energy harvesters [15–17], MEMS [18, 19], micro-accelerometers [20, 21] and biosensors [22, 23]. However piezoelectric-based structural vibration damping systems still remain one of the most investigated applications [24–27]

In order to mitigate the vibrations two systems can be implemented: passive and active. Passive systems are the most consolidated, the easiest to implement, low-cost and are usually based on resistive-inductive (R-L) shunt circuit. On the other hand they show a limited efficacy at low frequencies since high inductance is required (which is difficult to achieve) and a fine tuning of the parameters is necessary in the applications where the mode excited by the external load can change over time [28].

Active controls are the most efficient in applications where the resonant mode may vary over time because they can operate with larger bandwidth and can be tuned accordingly to the instantaneous load acting on the structure. On the other side, the active control systems require a power supply, an appropriate control algorithm and have higher costs.

With regards to the efficiency of active piezoelectric damping systems, the positioning and the size of the actuators are crucial. To this regard the optimal placement of piezoelectric actuators is typically represented by the detection of the minimum and/or maximum values of an objective function. As an example, the optimization criterion could be based on the maximization of: the modal forces or moments provided by the piezoelectric element, the deflection of the structure, the degree of observability or controllability of the desired modes, alternatively the minimization of the structure vibrations could be considered [29],[30]. Early studies by Crawley and De Luis [31] proposed the analytical solutions for the stress-strain relationships of piezoelectric single and patch actuators bonded on a beam. Furthermore it was pointed out that the actuators must be placed in the highest average strain areas to apply the maximum modal moments. The experimental evidence resulting from later studies [32],[33] seems to support this outcome. As a consequence, if the first flexural mode of a clamped-free beam is considered, the actuator should be placed as close as possible to the fixed end [34–36] while their optimal length coincides with the length of the beam. Such considerations have been extended to others constraint conditions as the simply supported beam. In fact it was shown by [37] that the piezoelectric actuators should be located in the zone between the nodal lines in order to obtain the highest damping effect. Barboni [38] showed that the piezoelectric actuators have to be placed within two consecutive zero curvature points when a single flexural mode of an Euler-Bernoulli beam has to be damped. Thereby, the optimal location of a collocated pair of actuators in order to damp the second flexural mode of a cantilever beam is obtained when the right edge of the actuators is on the free-end of the beam and the left edge is on the other zero curvature point (21.6% length of the beam away from the fixed end). A controllability index has also been proposed by [39] for two couples of Lead Zirconate Titanate (PZT) actuators in case of single and multimode vibrations of a beam.

Unfortunately, in many engineering applications the excited modes may be more than one at the same time, which can be the case of the turbomachinery rotor blades. In fact, the unsteady pressure due to the rotor-stator interaction may elicit two or more blade modes at certain shaft speeds. Several researchers studied the implementation of passive and active systems based on piezoelectric elements in order to damp this type of vibrations [40, 41]. However, the topic of the optimal positioning in case of multi-modal excitations has not been discussed as widely as the single modal excitation. Wang et al. [42] reported the optimal placement of anisotropic piezoelectric composite actuators to control single bending and twisting mode excitations and coupled flexural-torsional modes in a plate structure. In case of piezo-composite actuators the fiber orientation affects the damping efficiency, and the optimal orientation is different for bending and twisting modes, therefore a trade-off is required in case of coupled bending-twisting vibration. A semi-analytical model to optimize a sandwich type piezoelectric element in case of coupled bending-longitudinal excitations was proposed by [43].

Earlier works from the authors introduced an analytical method for the placement optimization of the piezoelectric actuators on a cantilever beam, in case of multiple simultaneously excited bending modes, and the outcomes were corroborated by numerical simulations [44, 45] and experimental results [46]. Recently the method has been improved by considering a piezoelectric bimorph beam entirely covered with several piezoelectric actuators couples, in such a way the optimization problem lies in the assessment of the optimal electric potential distribution that has to be provided to the actuators array, which maximizes the attenuation of the bi-modal excitations [47].

The behavior of a flexible beam that experiences the base motion is a topic of great interest because it is linked to aircraft rotors [48], spacecraft antennas [49], turbomachinery disc-blades coupled vibration [50–53] and to many other recent applications (e.g. energy harvesters) [54–56], so that it was widely investigated since 1940s. Vibration suppression in lightweight industrial robot manipulators is also a challenging problem when it comes to trajectory end-point control.

In fact the vibrations that arise from the motion of the robot arms may compromise the precision and speed of the manipulator. Several studies have been made on the control of the vibration induced by the base motion in cantilever structures by means of piezoelectric actuators [57–59].

In this paper a novel approach is proposed to analytically compute the position and the voltage amplitude required by the actuators in order to actively damp the vibrations of a cantilever piezoelectric bimorph beam, which is subjected to bi-modal excitations due to its support vibration. Here, the proposed method can be used to fully remove the beam elastic vibration, in fact only by knowing the pair of eigenfrequencies excited by the fixed-end motion, the designer can analytically calculate all the key parameters (voltage, size and position of the actuators). Moreover the solution is not unique, hence the parameters can be chosen on the basis of the specific application bounds. Below, the governing equations of motion are introduced and discussed. The analytical solutions have been compared with the numerical results obtained from FEM simulations performed with a commercial software (COMSOL) and a fair agreement appears. Furthermore, some applications are considered to show how the findings may help the designers to choose the proper set of material, size and location of piezoelectric actuators in cases where the full vibration suppression is desirable.

2. Materials and method

A cantilever beam is shown in Fig.1.

Figure 1: The cantilever beam under support vibration

Assuming that the fixed end is subjected to a support vibration $w^{\mathrm{s}}(t)$, this condition entails the rigid motion $w^{\mathrm{s}}(t)$ of the whole beam which in turn induces the vibration $w^{\mathrm{e}}(x,t)$. Thereby the total displacement $w(x,t)$ will be:

$$w(x,t) = w^{\mathrm{s}}(t) + w^{\mathrm{e}}(x,t) \tag{1}$$

In order to damp the vibrations $w^{\mathrm{e}}(x,t)$ the piezoelectric effect was used, so that two piezoelectric plates are surface bonded on the beam in a symmetrical position with respect to its axis (Fig.2). By a proper distribution of the electric potential, the opposite effect will be obtained; for example if the distribution in Fig.2 is considered, the upper plate stretches out while the bottom plate gets shorter.

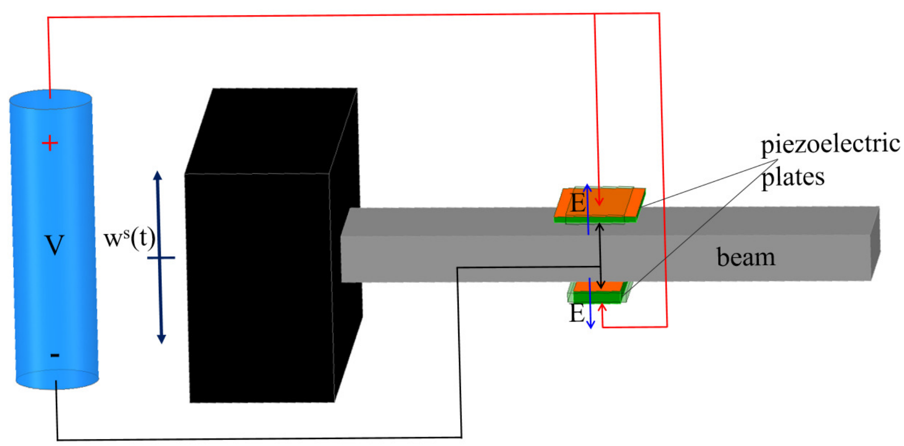

Figure 2: Example of potential distribution on piezoelectric plates (not in scale)

If such deformations are blocked, by gluing the plates on the beam, the piezoelectric internal stresses appear and stresses will be applied on the beam. It is possible to demonstrate that these stresses are concentrated at the ends of the piezoelectric plates [31] and their action is equivalent to two opposite flexural moments $M_{\mathrm{a}}(t)$ concentrated at their ends Fig. 3.

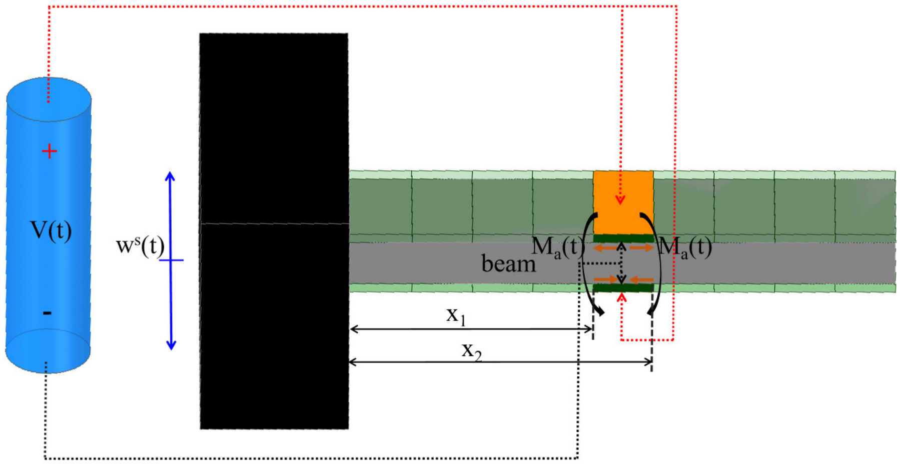

Figure 3: Actions of the piezoelectric plates on the beam (not in scale)

There are many research works in which these moments are used to damp the vibrations, however the actuators effectiveness strongly depends on the electric potential distribution and on their positioning. In this work, a model is proposed to find the most effective voltage and positions (x_1, x_2) to damp a single eigenmode or a combination of two eigenmodes, the results are compared with those obtained with a commercial FEM code (COMSOL).

Deriving the equilibrium equation by applying the principle of virtual work and naming the virtual work of elastic, inertial and piezoelectric forces respectively as δL_{e}, δL_{in}, and δL_{p}, the following can be written:

$$\delta L_{\mathrm{e}} = \delta L_{\mathrm{in}} + \delta L_{\mathrm{p}} \tag{2}$$

Denoting by a tilde the virtual quantities the individual terms are:

$$\delta L_{\mathrm{e}} = E_{\mathrm{b}} I_{\mathrm{b}} \int_0^{L_{\mathrm{b}}} \frac{\partial^2 w^{\mathrm{e}}}{\partial x^2} \frac{\partial^2 \widetilde{w}^{\mathrm{e}}}{\partial x^2} dx \tag{3}$$

$$\delta L_{\mathrm{in}} = -\rho S \int_0^{L_{\mathrm{b}}} \frac{\partial^2 w}{\partial t^2} \, \widetilde{w} \, dx \tag{4}$$

and δL_{p} (see Fig. 3)

$$\delta L_{\mathrm{p}} = M_{\mathrm{a}}\Big(\frac{\partial \tilde{w}^{\mathrm{e}}}{\partial x}|_{x=x_2} - \frac{\partial \tilde{w}^{\mathrm{e}}}{\partial x}|_{x=x_1}\Big) \tag{5}$$

where $M_{\mathrm{a}}(t)$ is (see [31]):

$$M_{\mathrm{a}}(t) = \frac{\psi}{6+\psi} E_{\mathrm{a}} b t_{\mathrm{a}} t_{\mathrm{b}} \Lambda(t) \tag{6}$$

and

$$\begin{cases} \psi = \frac{E_{\mathrm{b}} t_{\mathrm{b}}}{E_{\mathrm{a}} t_{\mathrm{a}}} \\ \Lambda(t) = \frac{d_{31}}{t_{\mathrm{a}}} V(t) \end{cases} \tag{7}$$

If $\phi_i(x)$ identifies the i-th natural mode of the cantilever beam, and $G_i(t)$ its corresponding normal coordinate, it is possible to state the elastic part of the displacement in the form:

$$w^{\mathrm{e}}(x,t) = \sum_{i=1}^{N} G_i(t)\phi_i(x) \tag{8}$$

while the virtual elastic displacement $\tilde{w}^{\mathrm{e}}$ part can be written as:

$$\tilde{w}^{\mathrm{e}} = C_j \phi_j(x) \tag{9}$$

Replacing the equations (3-9) in Eq. (2):

$$E_{\mathrm{b}} I_{\mathrm{b}} C_j \sum_{i=1}^{N} G_i(t) \int_0^{L_{\mathrm{b}}} \phi_i''(x)\phi_j''(x)dx = -\rho S C_j \sum_{i=1}^{N} \ddot{G}_i(t) \int_0^{L_{\mathrm{b}}} \phi_i(x)\phi_j(x)dx + \\ + M_{\mathrm{a}} C_j \Big[\phi_j'(x_2) - \phi_j'(x_1)\Big] - \rho S \ddot{w}^{\mathrm{s}}(x,t) C_j \int_0^{L_{\mathrm{b}}} \phi_j(x)dx \tag{10}$$

the Eq. 10 can be simplified considering the orthogonality of the principal modes and setting $C_j = 1$:

$$\ddot{G}_j(t) + \omega_j^2 G_j(t) = M_a \Big[\phi_j'(x_2) - \phi_j'(x_1)\Big] - \rho S \ddot{w}^{\mathrm{s}}(x,t) \int_0^{L_{\mathrm{b}}} \phi_j(x)dx \tag{11}$$

where ω_j are the natural angular frequencies of the beam.

Introducing the following quantities:

$$\begin{cases} \hat{M}_{\mathrm{a}} = \frac{M_{\mathrm{a}}}{V(t)} = \frac{\psi}{6+\psi} E_{\mathrm{a}} b t_{\mathrm{b}} d_{31} \\ Q_j = \rho S \int_0^{L_{\mathrm{b}}} \phi_j(x) dx \\ B_j(x_1, x_2) = \hat{M}_{\mathrm{a}} \left[\phi_j'(x_2) - \phi_j'(x_1) \right] \end{cases} \tag{12}$$

the Eq. (11) simplifies into:

$$\ddot{G}_j(t) + \omega_j^2 G_j(t) = B_j(x_1, x_2) V(t) - \ddot{w}^{\mathrm{s}}(t) Q_j \tag{13}$$

or, if the Rayleigh damping $\mathbf{C} = \alpha \mathbf{M} + \beta \mathbf{K}$ is included, turns into:

$$\ddot{G}_j(t) + (\alpha + \beta \omega_j^2) \dot{G}_j(t) + \omega_j^2 G_j(t) = B_j(x_1, x_2) V(t) - \ddot{w}^{\mathrm{s}}(t) Q_j \tag{14}$$

From the solution of the Eq. (14) the dynamic behavior of the beam is obtained. In the second member it is possible to distinguish the exciting effect due to the vibration support w^{s} and the contribute of the piezoelectric plates $B_j(x_1, x_2)V(t)$.

High amplitude vibrations can occur when the support vibrates at frequencies close to one or more eigenfrequencies of the beam with all the related problems. In order to study this critical condition the following general expression for $w^{\mathrm{s}}(t)$ was chosen:

$$w^{\mathrm{s}}(t) = \sum_{k=1}^{N_{\mathrm{s}}} A_k \cos(\omega_k t) \tag{15}$$

where N_s is the number of the excited modes, while A_k is the vibration amplitude of the support at the k-th eigenfrequency. The strategy used in this work to damp such vibrations, that is typical for the active damping methods, relies on using the piezoelectric plates to induce counter-vibrations (i.e. in phase opposition) at the same frequencies of the vibration induced by $w^{\mathrm{s}}(t)$ in such a way as to cancel or reduce it. To this regard the following expression for the voltage $V(t)$ has been chosen:

$$V(t) = \sum_{k=1}^{N_\mathrm{s}} V_k \cos(\omega_k t) \tag{16}$$

which replaced in Eq. (14) gives:

$$\begin{aligned} &\ddot{G}_j\ (t) + (\alpha + \beta\omega_j^2)\ \dot{G}_j\ (t) + \omega_j^2 G_j(t) = \\ &= \sum_{k=1}^{N_\mathrm{s}} \Big[B_j(x_1, x_2) V_k(t) + \omega_k^2 A_k Q_j \Big] \cos(\omega_k t) \end{aligned} \tag{17}$$

In [45] has been shown that, for $\beta = 0$ and $w^\mathrm{s}(t) = 0$, the solution of Eq. (17) is:

$$G_j(t) = \frac{B_j(x_1, x_2) V_j \sin(\omega_j t)}{\alpha\omega_j} \tag{18}$$

Generalizing the solution for a cantilever beam attached to a moving base and $\beta \neq 0$ the ampitude of G_j can be written:

$$G_j = \frac{\big[B_j(x_1, x_2) V_j + \omega_i^2 A_j Q_j \big]}{\alpha\omega_j + \beta\omega_j^3} \tag{19}$$

and Eq. (8) becomes:

$$w^\mathrm{e}(x,t) = \sum_{j=1}^{N_\mathrm{s}} \frac{\big[B_j(x_1, x_2) V_j + \omega_i^2 A_j Q_j \big]}{\alpha\omega_j + \beta\omega_j^3} \sin(\omega_j t) \phi_j(x) \tag{20}$$

In the literature several methods are used to evaluate the effectiveness of a damping system but, in case of cantilever structures, the tip displacement is commonly used as a reference point to assess the damping system effectiveness [60–62]. The method proposed in this paper benefits from the feature that every eigenmode of the cantilever beam has its maximum amplitude at the free end. Therefore, if an eigenmode is excited this point will have the maximum vibration amplitude. Similarly, if its vibration amplitude is reduced the amplitude of the all the other points is also reduced. Therefore, the vibration amplitude of the free end was chosen to evaluate the actuation efficiency of the PZT actuators. Considering Eq. (8) and Eq. (19) this will be:

$$|w_L^{\mathrm{e}}(x_1,x_2)| = \sum_{i=1}^{N_{\mathrm{s}}} \Big| \frac{\big[B_i(x_1,x_2)V_i + \omega_i^2 A_i Q_i\big]\phi_i(L)}{\alpha\omega_i + \beta\omega_i^3} \Big| \tag{21}$$

In this work the support vibration may excite one eigenmode or two eigenmodes simultaneously. Hence the parameter r ($0 \le r \le 1$) is introduced to take into account how the excitation is distributed between the two eigenmodes. So that, indicating with A a reference amplitude and with i_1, i_2 the indexes of the excited modes, $w^{\mathrm{s}}(t)$ can be written in the form:

$$w^{\mathrm{s}}(t) = A\big[(1-r)\cos(\omega_{i_1}t) + r\cos(\omega_{i_2}t)\big] \tag{22}$$

Interesting results are obtained when $V(t)$ is chosen with a spectrum similar to that of the $w^{\mathrm{s}}(t)$:

$$V(t) = V\big[(1-r)\cos(\omega_{i_1}t) + r\cos(\omega_{i_2}t)\big] \tag{23}$$

In fact replacing Eq. (23) in Eq. (21) the amplitude $|w_L^{\mathrm{e}}(x_1,x_2)|$ turns into the following simplified form:

$$\begin{aligned} |w_L^{\mathrm{e}}(x_1,x_2)| = &\Big| \frac{\big[B_{i_1}(x_1,x_2)V + \omega_{i_1}^2 A Q_{i_1}\big](1-r)\phi_{i_1}(L)}{\alpha\omega_{i_1} + \beta\omega_{i_1}^3} \Big| + \\ &+ \Big| \frac{\big[B_{i_2}(x_1,x_2)V + \omega_{i_2}^2 A Q_{i_2}\big] r\phi_{i_2}(L)}{\alpha\omega_{i_2} + \beta\omega_{i_2}^3} \Big| \end{aligned} \tag{24}$$

or by explicating the vector $\mathbf{B}$:

$$\begin{aligned} |w_L^{\mathrm{e}}(x_1,x_2)| = &\Big| \Big\{ \frac{\hat{M}_{\mathrm{a}} \big[\phi'_{i_1}(x_2) - \phi'_{i_1}(x_1)\big]V + \omega_{i_1}^2 A Q_{i_1}}{\alpha\omega_{i_1} + \beta\omega_{i_1}^3} \Big\} (1-r)\phi_{i_1}(L) \Big| + \\ &+ \Big| \Big\{ \frac{\hat{M}_{\mathrm{a}} \big[\phi'_{i_2}(x_2) - \phi'_{i_2}(x_1)\big]V + \omega_{i_2}^2 A Q_{i_2}}{\alpha\omega_{i_2} + \beta\omega_{i_2}^3} \Big\} r\phi_{i_2}(L) \Big| \end{aligned} \tag{25}$$

In order to have $|w_L^{\mathrm{e}}(x_1, x_2)| = 0$ it is sufficient to put equal to zero, individually, the two addends:

$$\begin{cases} \hat{M}_{\mathrm{a}} \left[\phi'_{i_1}(x_2) - \phi'_{i_1}(x_1)\right] V + \omega_{i_1}^2 A Q_{i_1} = 0 \\ \hat{M}_{\mathrm{a}} \left[\phi'_{i_2}(x_2) - \phi'_{i_2}(x_1)\right] V + \omega_{i_2}^2 A Q_{i_2} = 0 \end{cases} \tag{26}$$

From the previous system it is possible to calculate the voltage V from one of the two equations and the position (x_1, x_2) of the piezoelectric plates from the other. For example calculating V from the first:

$$V(i_1, A, x_1, x_2) = -\frac{\omega_{i_1}^2 A Q_{i_1}}{\hat{M}_{\mathrm{a}} \left[\phi'_{i_1}(x_2) - \phi'_{i_1}(x_1)\right]} \tag{27}$$

and replacing it in Eq. (26).2 leads to the equation:

$$f(i_1, i_2, x_1, x_2) = \omega_{i_2}^2 Q_{i_2} \left[\phi'_{i_1}(x_2) - \phi'_{i_1}(x_1)\right] - \omega_{i_1}^2 Q_{i_1} \left[\phi'_{i_2}(x_2) - \phi'_{i_2}(x_1)\right] = 0 \tag{28}$$

from which x_1 and x_2 can be calculated.

Anyway if just one mode is excited ($r = 0$), Eq. (25) becomes:

$$|w_L^{\mathrm{e}}(x_1, x_2)| = \left| \left\{ \frac{\hat{M}_{\mathrm{a}} \left[\phi'_{i_1}(x_2) - \phi'_{i_1}(x_1)\right] V + \omega_{i_1}^2 A Q_{i_1}}{\alpha \omega_{i_1} + \beta \omega_{i_1}^3} \right\} \phi_{i_1}(L) \right| \tag{29}$$

and only Eq. (27) needs to be verified to obtain $|w_L^{\mathrm{e}}(x_1, x_2)| = 0$.

3. Results and discussions

In this section the analytical results of the proposed model are compared with the FEM simulations. The material and overall dimensions of the beam and piezoelectric actuators considered in the simulations are reported in Table (1) while the amplitude A was set to 0.1 mm. The dimensionless coordinates $\xi_1 = \frac{x_1}{L}$ and $\xi_2 = \frac{x_2}{L}$ will be used to indicate the positions of the left and right edges of the piezoelectric actuators.

Table 1: Material and geometrical properties

	Steel	**PZT-5A**
Mass density [kg/m^3]	7.85×10^3	7.75×10^3
Young modulus [N/m^2]	200×10^9	69.3×10^9
Poisson ratio	0.33	-
$\mathbf{d_{31}}$[C/N]	-	-1.71×10^{-10}
Length [mm]	800	34.78
Width [mm]	30	30
Thickness [mm]	3	0.5

The piezoelectric plates can provide a damping effect if an electric circuit like the one described hereinafter may be considered. Fig.4 shows the outline of a feasible experimental setup where 23 pairs of PZT actuators were considered. The function generator delivers a sinusoidal voltage $\mathrm{v_f}(t)$ or, in case of bi-modal excitation, a periodic voltage consisting of two frequencies. The signal is then magnified by a γ factor by means of an amplifier in non-inverting configuration supplied with a dual voltage $\pm V_{\mathrm{cc}}$. The amplifier is essential since the considered piezoelectric plates may be supplied with a voltage such high as 250 V - 300 V and a commercial function generator typically provides up to $\pm$20 V. The amplified voltage is then delivered to all the external electrodes of each actuator while the voltage on the internal electrodes must be phase-shifted by 180 degrees, therefore 23 inverting buffers have been included in order to provide the output voltage $-\gamma \mathrm{v_f}(t)$. This system allows to use 23 relays in order to selectively deactivate one or more PZT pairs depending on the values of (x_1, x_2) used to damp the considered vibration. The relays can be controlled by an analog or digital signal from an external microcontroller such as in [63].

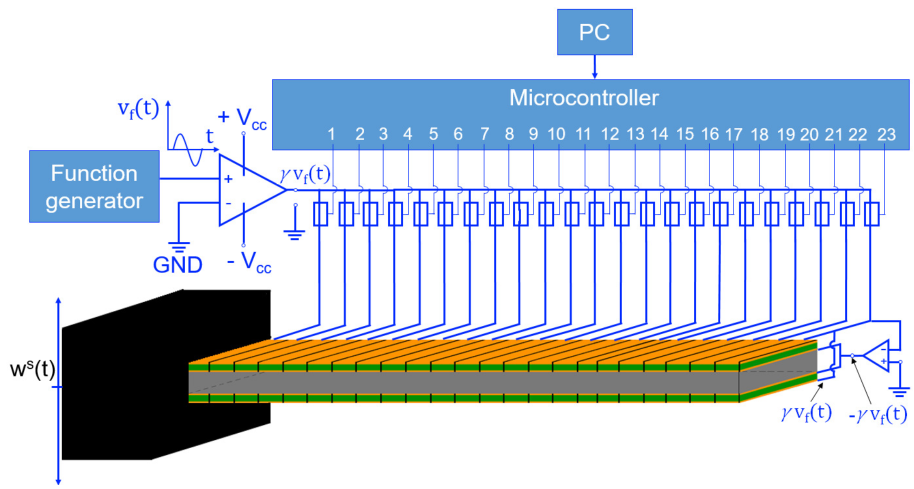

Figure 4: The electric circuit to drive the piezoelectric actuators. $1, 2, 3, ..., 23$ represent the digital outputs (DO) of a microcontroller which handles 23 mechanical relays. Each DO can be set as: High (H, closed circuit) or Low (L, open circuit).

3.1. Single mode excitations

In this paragraph, the cases of single mode excitations will be seen and the first five eigenmodes will be addressed. From Eq. (27), for every eigenmode, the electric potential V that allows to reach $w_L^{\mathrm{e}} = 0$ has been calculated. The equation shows that the action of the piezoelectric actuators depends on the position of the edges of the plates (see also Eq. (5)): the effectiveness of this action will increase as the difference $\phi'_{i_1}(\xi_2) - \phi'_{i_1}(\xi_1)$ increases or, in other words, the larger is the difference $\phi'_{i_1}(\xi_2) - \phi'_{i_1}(\xi_1)$ the lower is the voltage needed to suppress the elastic vibration ($w_L^{\mathrm{e}} = 0$). In Figs. 5a - 9a the plots of the derivatives of the first five modes have been reported. Each derivative has its absolute maximum in $\xi_2 = 1$, while the position of the absolute minimum depends on the considered mode. Such position has been highlighted with the dashed red lines and the difference $\phi'_{i_1}(\xi_{\max}) - \phi'_{i_1}(\xi_{\min})$ has been represented with the red arrows. For every eigenmode the blue rectangle represents the best efficiency position of the piezoelectric plates to damp that mode. In Figs. 5b - 9b the corresponding configuration of the electrical circuit are also reported:

the active piezoelectric plates are depicted in orange and the inactive ones in gray.

In order to verify the proposed model, for each excited mode, the values $\xi_{\max}$, $\xi_{\min}$ and V were computed from Eq. (27) and were used in a FEM software to obtain w_L versus time t (Figs. 5c - 9c). To highlight the damping efficacy, the instant from which the piezoelectric action begins has been set to $t_0 \neq 0$. The activation of the actuators can be seen to cause a fast decrease of $|w_L|$ and, substantially, only w^{s} remains. To prove that the damped vibrations of the free end imply the damping of the whole beam vibrations, the maximum value of the mean of $|w(x,t)|$:

$$\overline{w_{\mathrm{m}}(t)} = \frac{1}{L_{\mathrm{b}}} \int_0^{L_{\mathrm{b}}} |w(x,t)| dx \tag{30}$$

has been calculated and compared as to two conditions (without and with control) by means of FEM analysis[1]. It can be observed that the proposed method is effective to damp the vibrations of the whole beam for all the configurations taken into account (Figs. 5d - 9d).

3.2. Bi-modal excitations

Following a closer analysis of equations (27) and (28), it can be noted that the values of (ξ_1, ξ_2) and V are affected only by the indexes of the excited modes (i_1, i_2) while the modes coupling ratio r has no influence, so that once the coupled modes are identified, if any change in the spectral distribution between the two eigenmodes occurs, it is not necessary to change the control parameters. In case of vibration damping in gas turbines rotor blades, for example, the bi-modal excitations may vary in accordance with both the shaft speed and the degree of mistuning of the blades. In fact, the mistuning may

[1] The mean value $\overline{w_{\mathrm{m}}(t)}$ is proportional to the amplitude vibrations of the whole beam. It depends on time and for every regime (damped or not damped) has been selected the instant where this value is maximum in order to compare the two configurations in equivalent conditions.

cause the onset of excessive vibrations in one or more blades of the bladed disk and the coupling ratio of the eigenfrequencies involved may vary from blade to blade. This implies that some blades might be excited with different values of r, nevertheless a vibration damping system based on the proposed method would not be sensitive to this issue.

The results obtained for several bi-modal excitations are reported in Figs. 10 - 17. The solutions of the Eq. (28) are reported in Figs. 10a - 17a, while (b), (c) and (d) plots show w_L versus time, calculated for the same control parameters (ξ_1, ξ_2, V) but different r values, by means of a COMSOL FEM code. As it may be noted, several solutions (ξ_1, ξ_2) are available for each pair of coupled modes (i_1, i_2) but these differ from each other for their efficiency or, in other words, for the voltage needed to achieve the same result. The adopted procedure was the following: first the indexes of the coupled modes i_1, i_2 were chosen, then the values of (ξ_1, ξ_2) were calculated by solving Eq. (28) and choosing, among all the available solutions, the most efficient as the one which requires the lowest voltage V value. Thereafter, these values were included in the COMSOL FEM code to perform the dynamic analysis. The piezoelectric actuators were activated after 1 second from the beginning. Different r values were chosen to corroborate the model in different conditions. The effectiveness of the piezoelectric active damping can clearly be seen, in fact after its activation only the displacement w^{s} remains, while the elastic displacement w_L^{e} is almost completely suppressed. In Figs. 10c - 17c the configurations with the maximum value of the mean of $|w(x,t)|$, obtained with a FEM analysis as previously done for the single mode excitations, are reported. Even in case of bi-modal excitations the efficiency of the proposed method for damping the vibrations of the whole beam can be observed.

One of the advantages of the proposed method is that for each bi-modal excitation different set of pairs (ξ_1, ξ_2), with the corresponding V, are available to completely attenuate the elastic part of the vibration, and this simplifies the problem of the optimal positioning of the actuators for the following reasons:

1. if the particular application involves a unique bi-modal excitation which must be addressed, the designer can select the optimal (ξ_1, ξ_2) on the basis of the project bonds (maximum admissible piezoelectric voltage, costs, dimensions, etc.);
2. if the application requires the damping of different bi-modal excitations (for example simultaneously synchronous resonances occurring in bladed assemblies [64–66]) the structure may be covered with multiple pairs of actuators (up to the full coverage of the structure in the most general case), so that the only additional complication is the proper powering of the group of actuators that allows to mitigate the ongoing excitation.

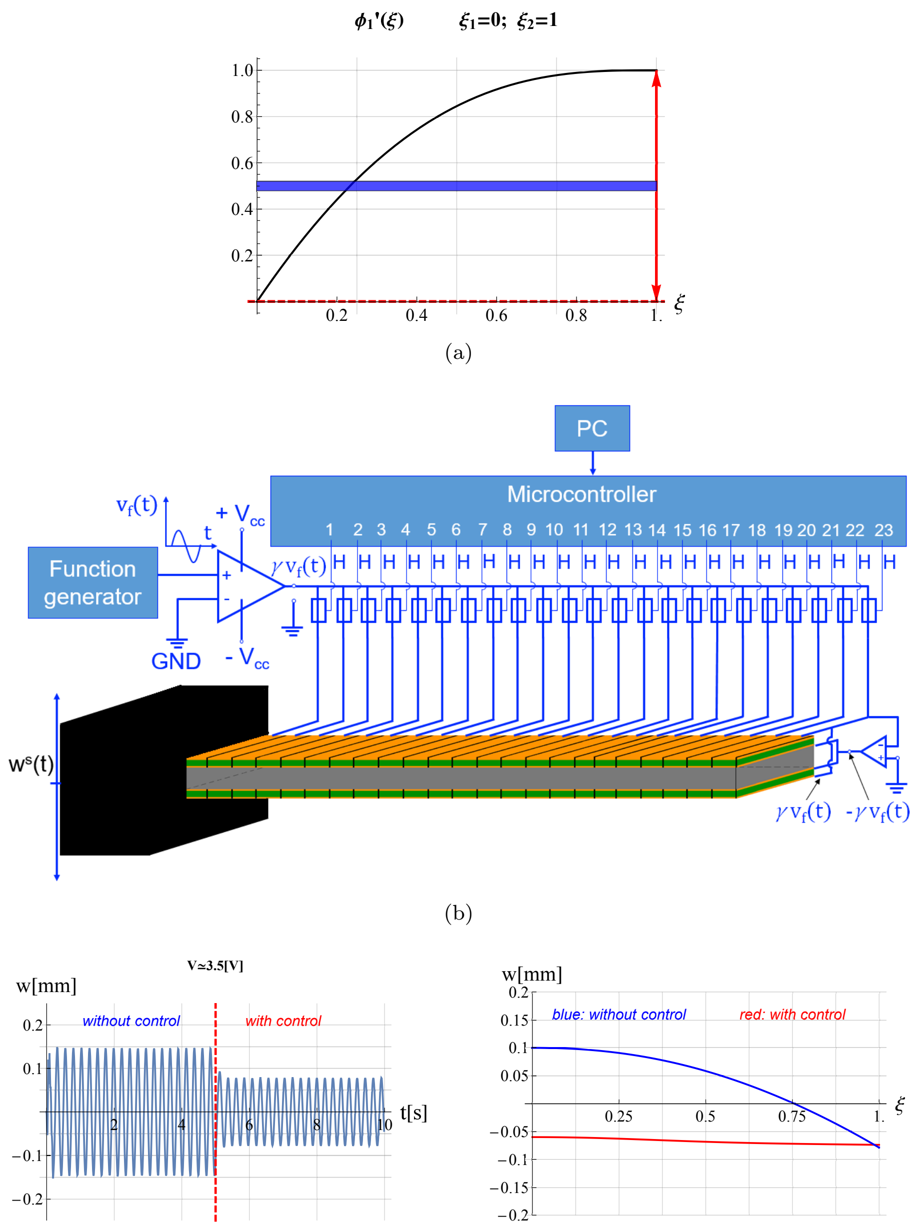

Figure 5: (a) the derivative of the first eigenmode (solid black line) and the illustration of the most efficient position of the piezoelectric plates (blue rectangle); (b) the corresponding circuital scheme; (c) and (d), respectively, the plot of w_L vs t and the configuration (without and with control), to which the maximum value of the mean of $|w(x,t)|$ corresponds, both calculated by means of the COMSOL FEM code considering the data obtained by the proposed model and reported in the label of the plot.

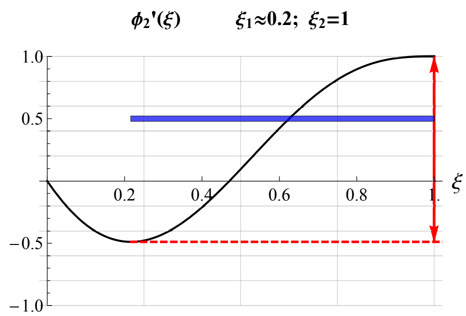

(a)

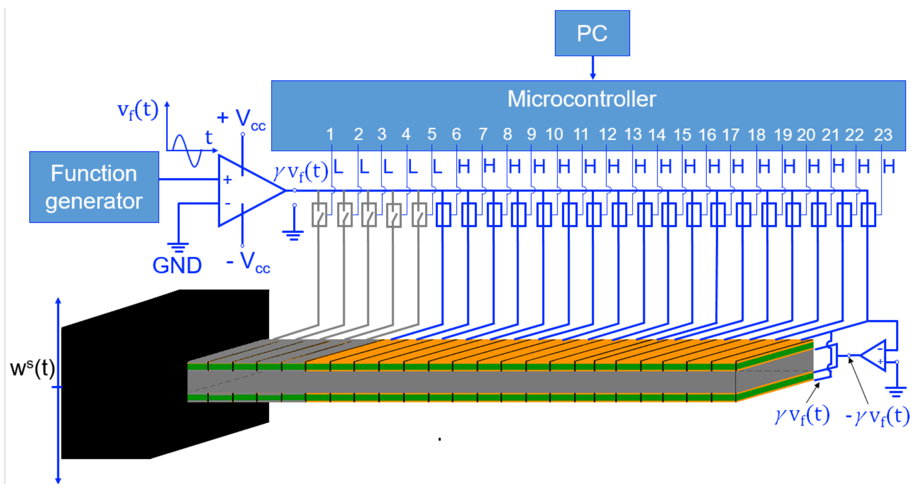

(b)

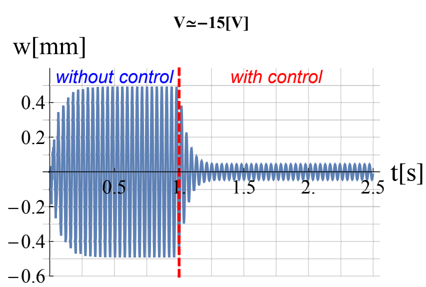

(c)

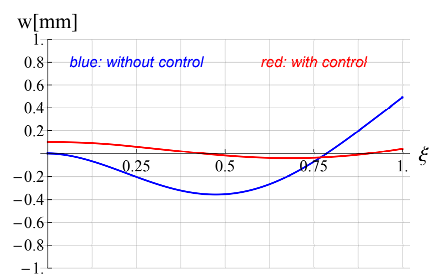

(d)

Figure 6: The second flexural mode is considered here. (a), (b), (c), (d) have the same meaning as in Fig. 5.

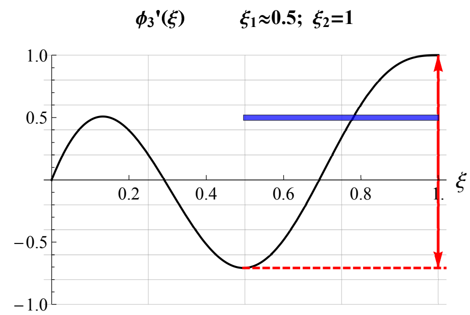

(a)

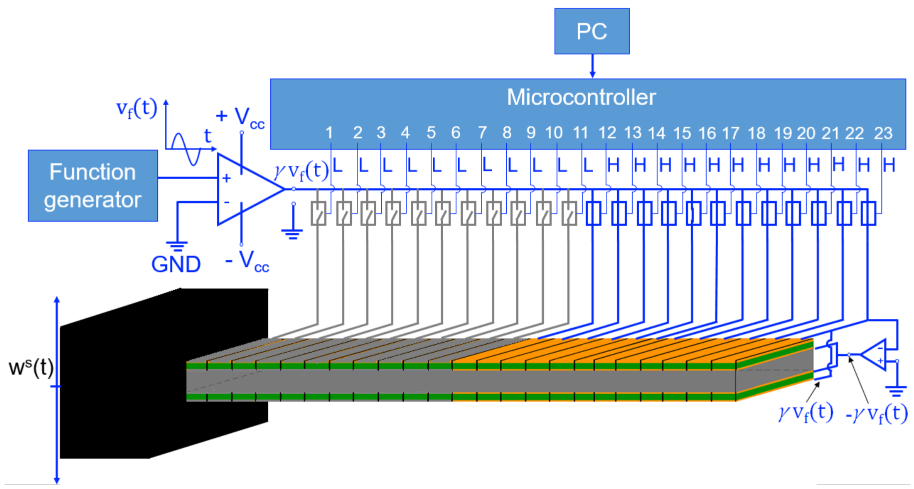

(b)

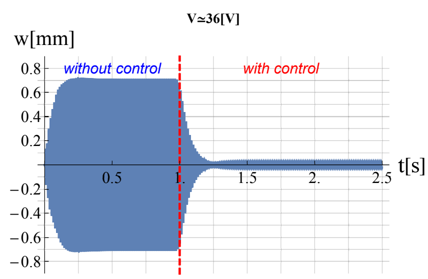

(c)

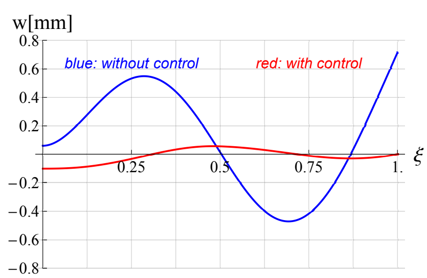

(d)

Figure 7: The third flexural mode is considered here. (a), (b), (c), (d) have the same meaning as in Fig. 5.

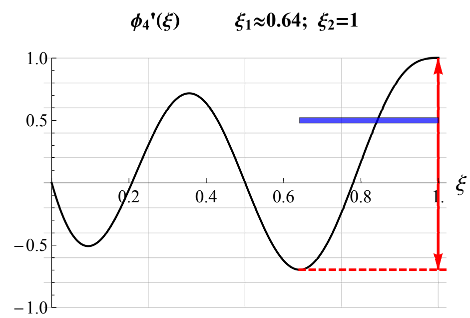

(a)

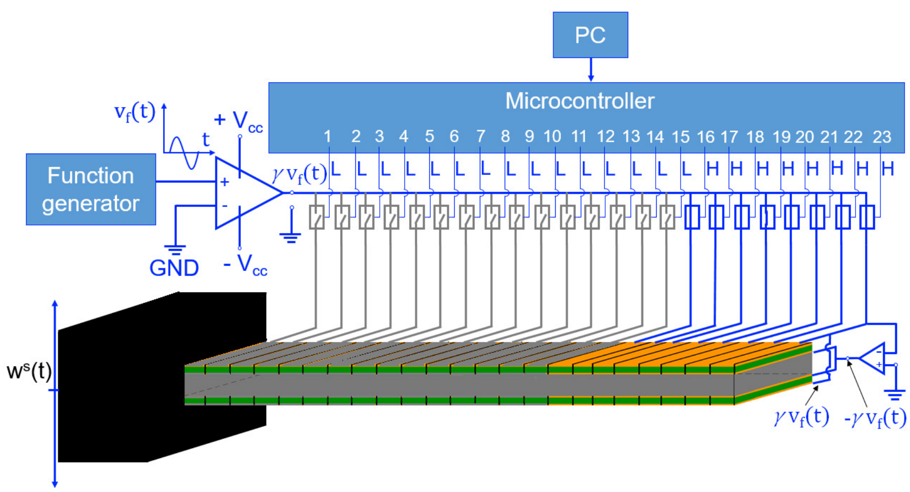

(b)

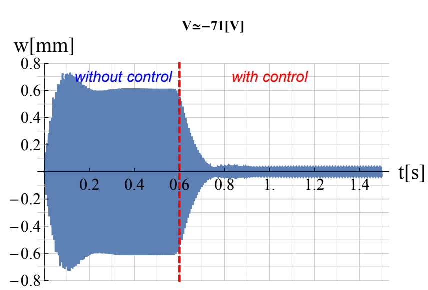

(c)

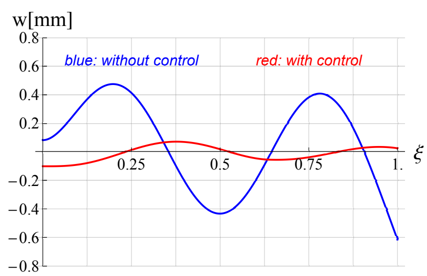

(d)

Figure 8: The fourth flexural mode is considered here. (a), (b), (c), (d) have the same meaning as in Fig. 5.

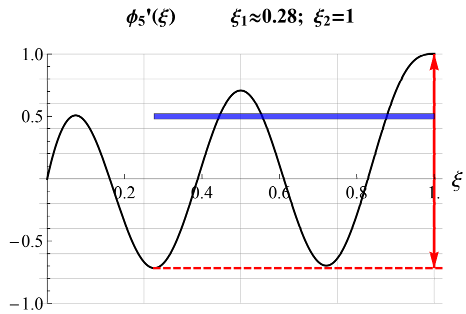

(a)

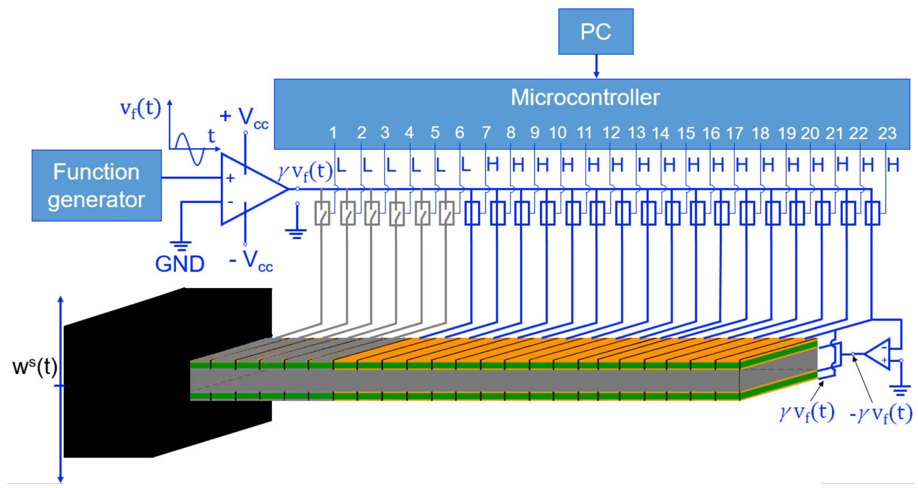

(b)

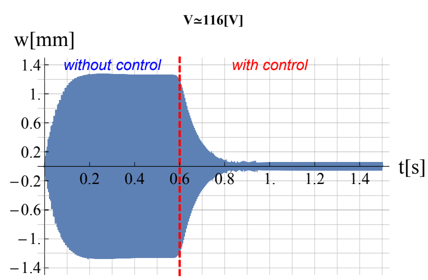

(c)

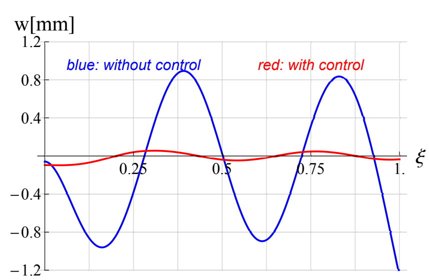

(d)

Figure 9: The fifth flexural mode is considered here. (a), (b), (c), (d) have the same meaning as in Fig. 5.

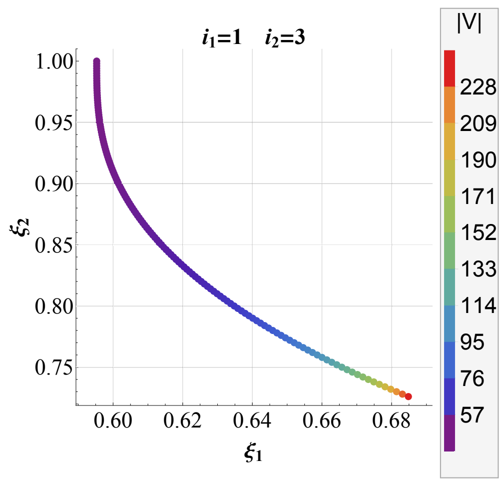

(a)

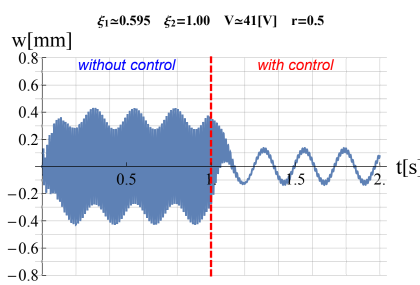

(b)

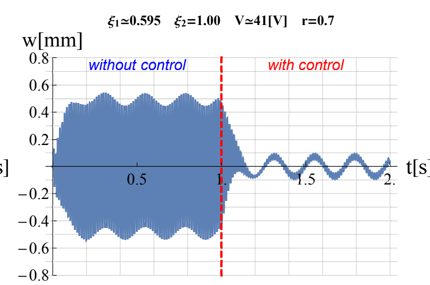

(c)

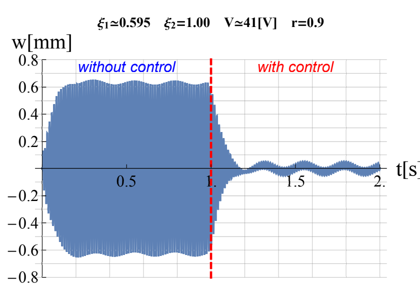

(d)

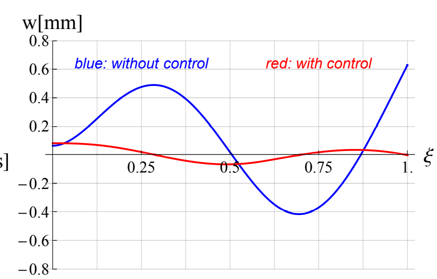

(e)

Figure 10: The first and the third coupled modes are considered. In (a) the plot of the solution couples $\{\xi_1, \xi_2\}$ calculated from the Eq. (28); in (b),(c) and (d) the plots of w_L vs t obtained for the same configuration $(\{\xi_1, \xi_2\}, V)$ but different r values; in (e) the configuration (without and with control), to which the maximum value of the mean of $|w(x,t)|$ corresponds, both calculated by means of the COMSOL FEM code considering the data obtained by the proposed model and reported in the label of the plot. The (e) plot is the same for every r values of (b),(c),(d) plots.

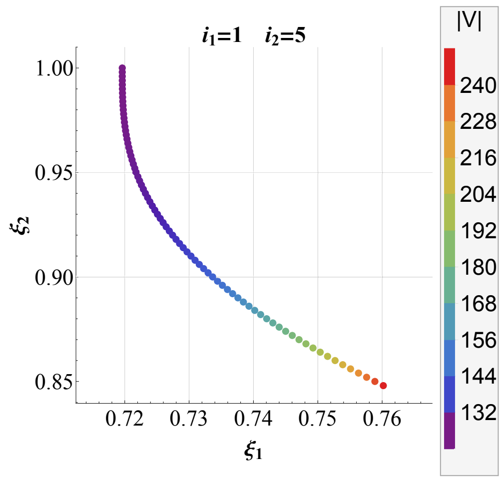

(a)

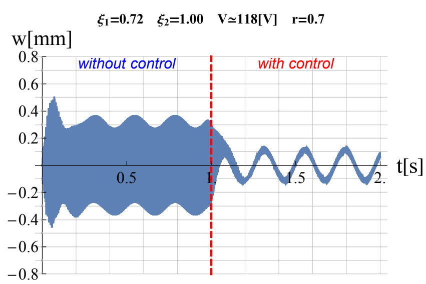

(b)

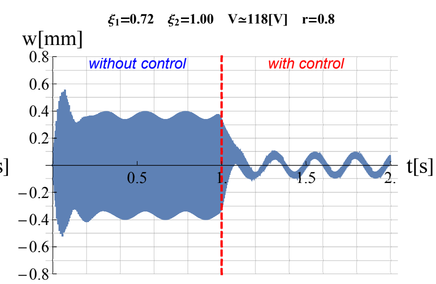

(c)

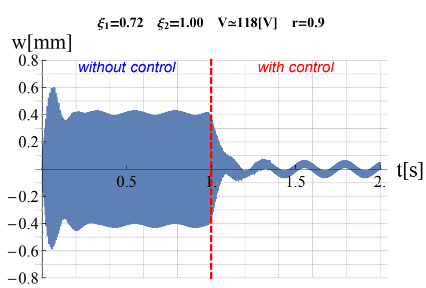

(d)

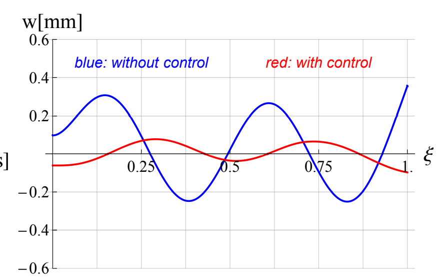

(e)

Figure 11: The first and fifth coupled modes are considered here. (a), (b), (c), (d), (e) have the same meaning as in Fig. 10.

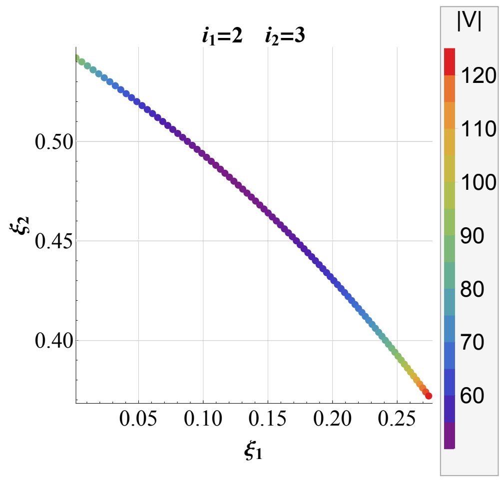

(a)

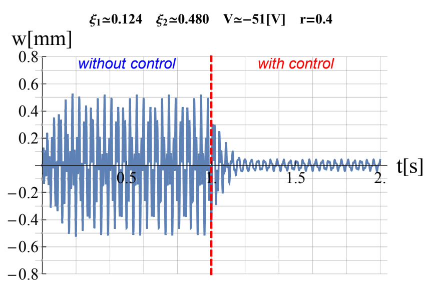

(b)

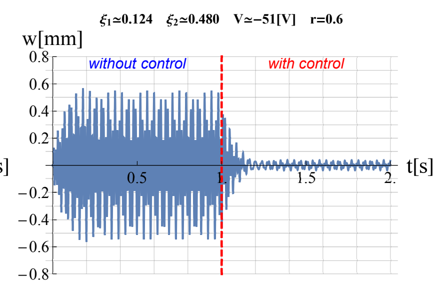

(c)

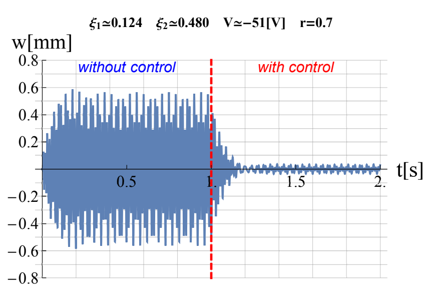

(d)

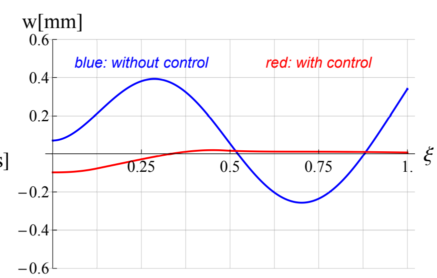

(e)

Figure 12: The second and third coupled modes are considered here. (a), (b), (c), (d), (e) have the same meaning as in Fig. 10.

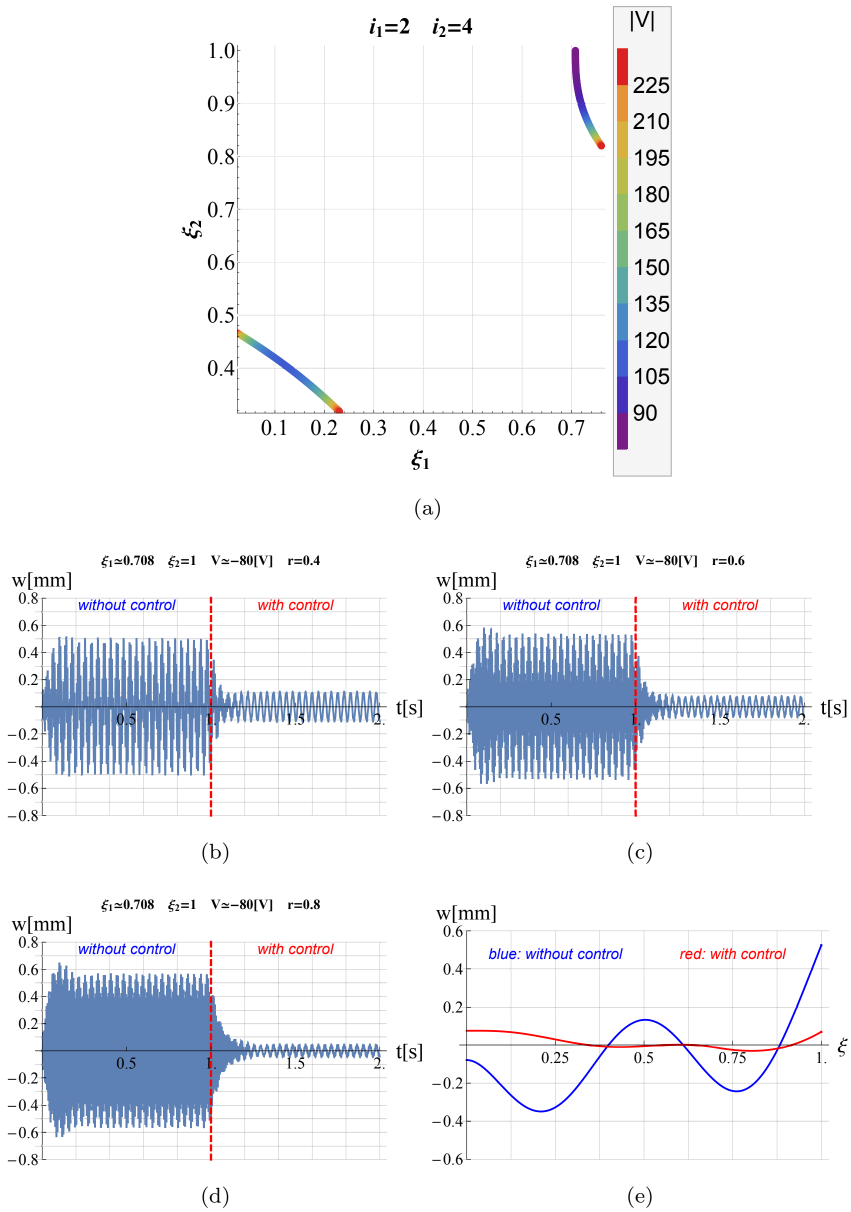

Figure 13: The second and fourth coupled modes are considered here. (a), (b), (c), (d), (e) have the same meaning as in Fig. 10.

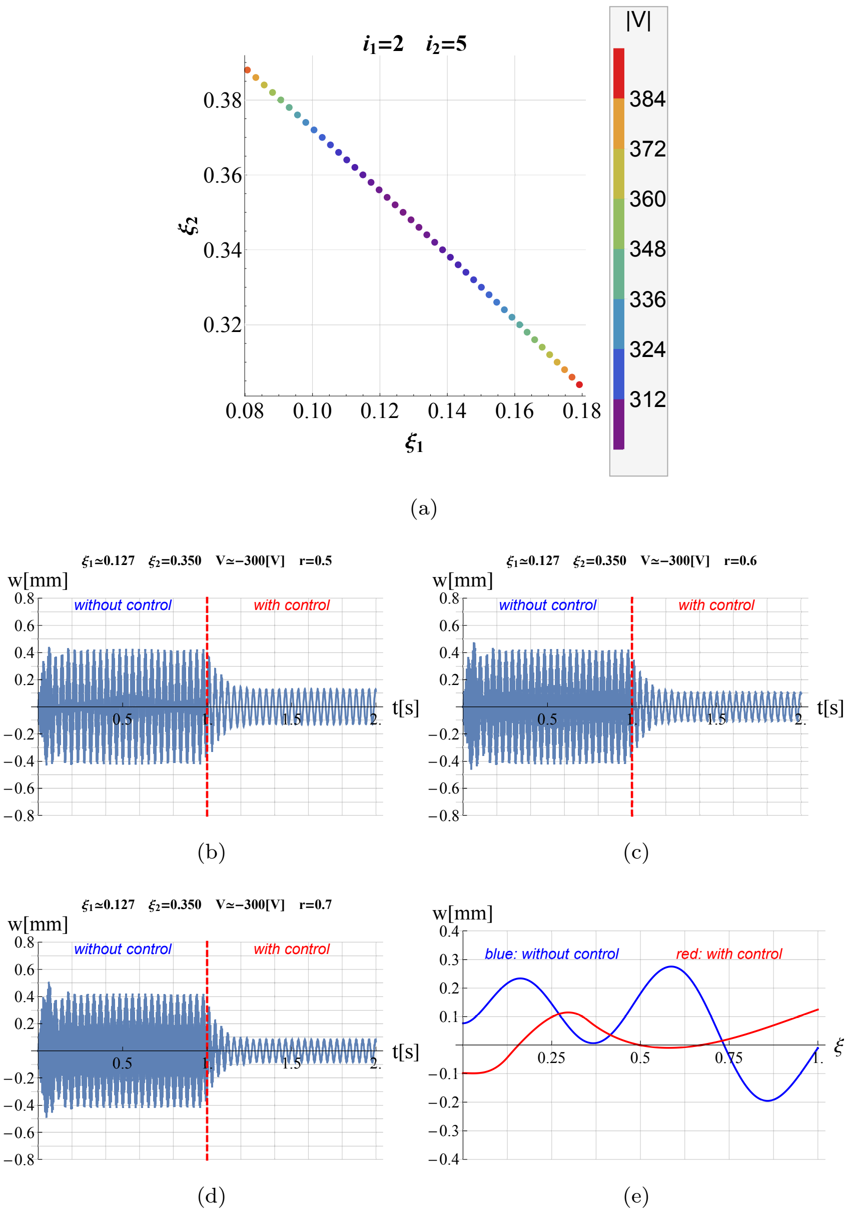

Figure 14: The second and fifth coupled modes are considered here. (a), (b), (c), (d), (e) have the same meaning as in Fig. 10.

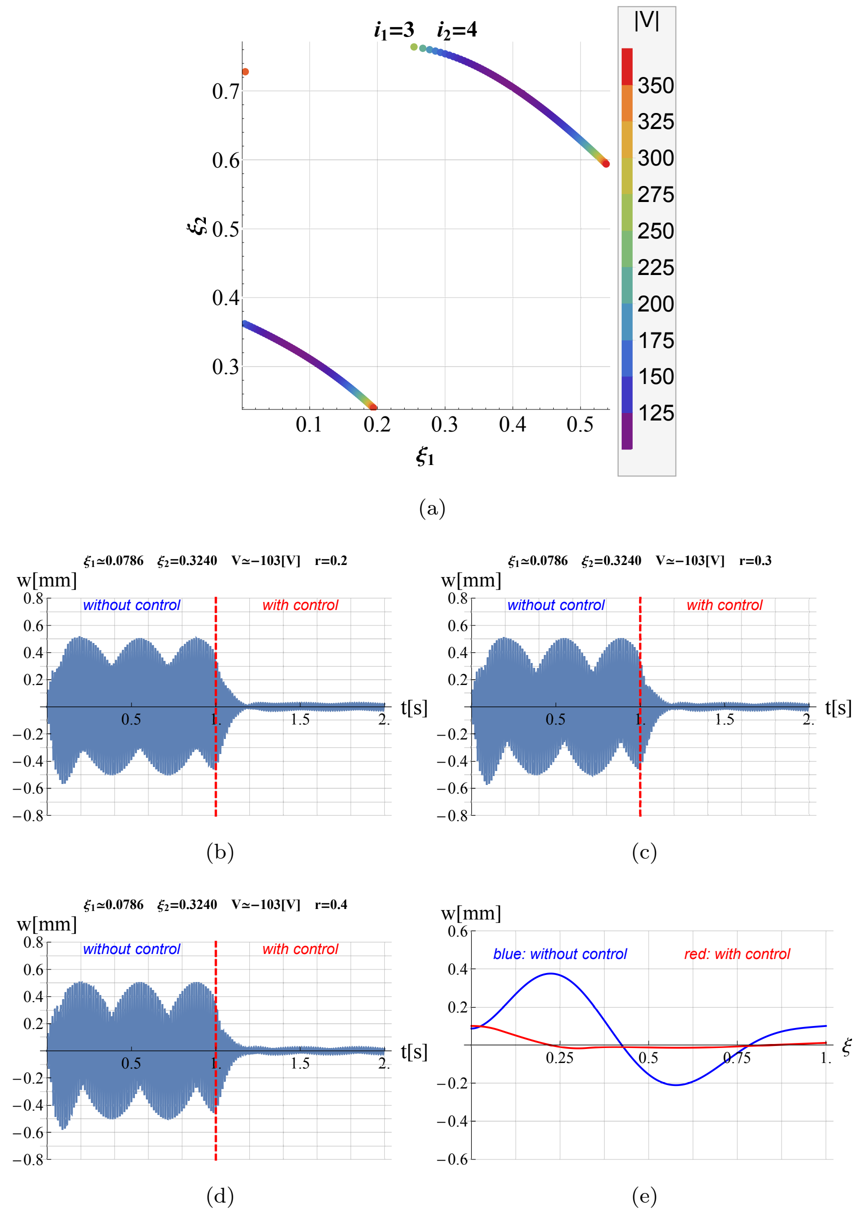

Figure 15: The third and fourth coupled modes are considered here. (a), (b), (c), (d), (e) have the same meaning as in Fig. 10.

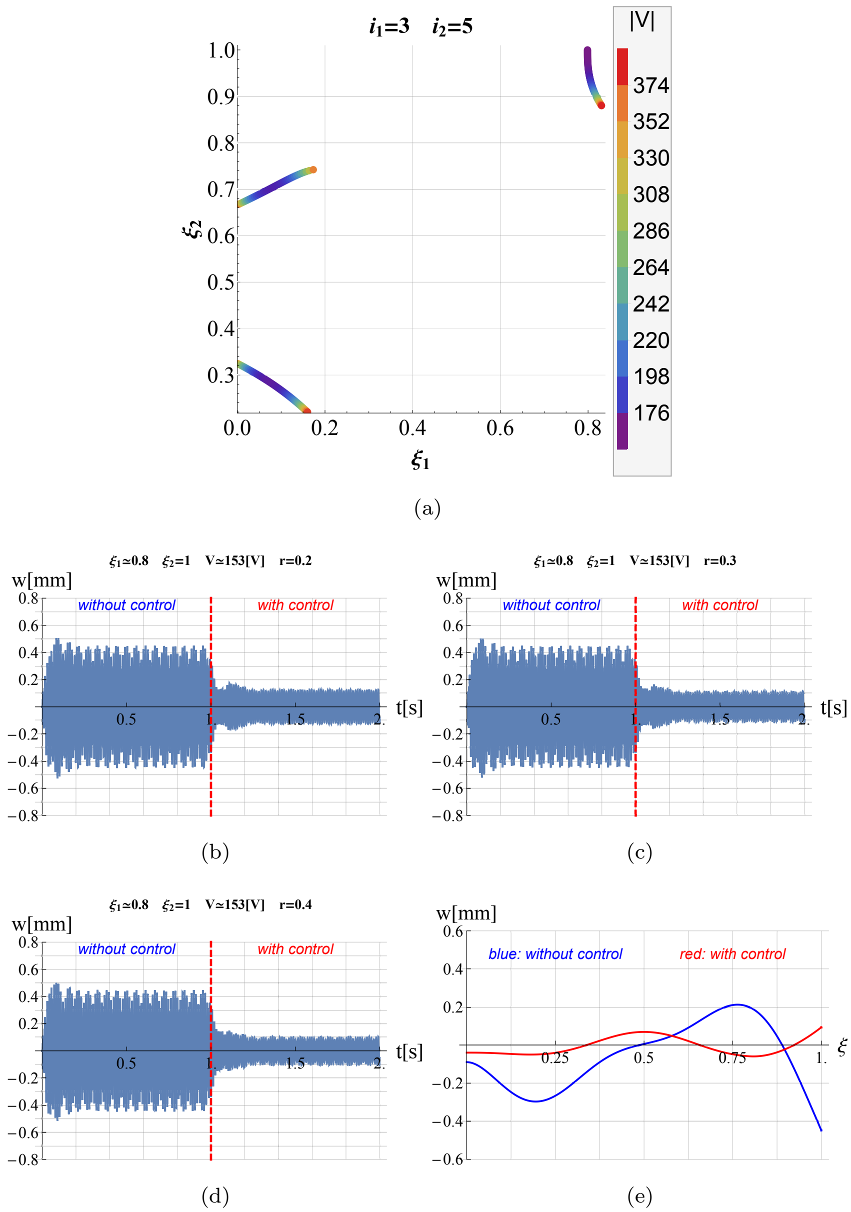

Figure 16: The third and fifth coupled modes are considered here. (a), (b), (c), (d), (e) have the same meaning as in Fig. 10.

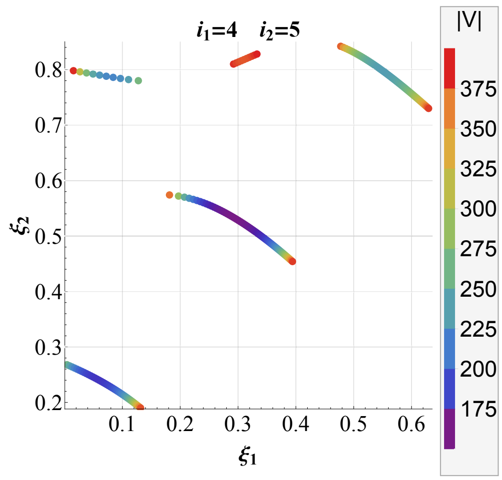

(a)

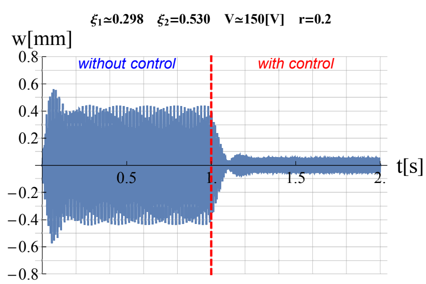

(b)

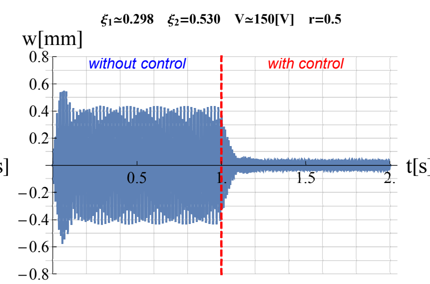

(c)

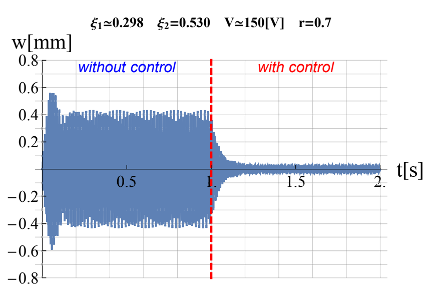

(d)

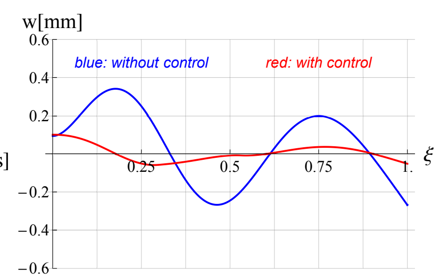

(e)

Figure 17: The fourth and fifth coupled modes are considered here. (a), (b), (c), (d), (e) have the same meaning as in Fig. 10.

4. Conclusions

In this paper a new model to damp the elastic vibrations induced in a cantilever beam by the support vibration is proposed. An active damping system based on the piezoelectric actuators has been considered. The innovation of this research consists in the provision of a new formula that allows to concurrently identify both the best actuators placement and the proper electric potential that must be applied to the actuators, regardless of the degree of modes coupling. As a consequence, depending on both the nature of the application and the number of bi-modal excitations which have to be addressed, designers can figure out the overall dimensions of the piezoelectric actuators, calculate the required power and their related costs. With the aim of corroborating the proposed analytical model, a comparison with the results obtained by means of a FEM software was performed and a good agreement was found between the analytical and numerical model results.

References

[1] M. B. Xu, G. Song, Adaptive control of vibration wave propagation in cylindrical shells using sma wall joint, J. Sound. Vib. 278 (2004) 307–326. doi:10.1016/j.jsv.2003.10.029.

[2] N. D. Tiwari, A. Gogoi, B. Hazra, Q. Wang, A shape memory alloy-tuned mass damper inerter system for passive control of linked-sdof structural systems under seismic excitation, J. Sound. Vib. 494 (2021) 115893. doi:10.1016/j.jsv.2020.115893.

[3] K. A. Williams, G. T.-C. Chiu, R. J. Bernhard, Dynamic modelling of a shape memory alloy adaptive tuned vibration absorber, J. Sound. Vib. 280 (2005) 211–234. doi:10.1016/j.jsv.2003.12.040.

[4] S. R. Hong, S. B. Choi, Y. T. Choi, N. M. Wereley, A hydro-mechanical model for hysteretic damping force prediction of er damper: experimental verification, J. Sound. Vib. 285 (2005) 1180–1188. doi:10.1016/j.jsv.2004.10.031.

[5] A. S. Tan, J. Aramendiz, K. H. Ross, T. Sattel, A. Fidlin, Comparative study between dry friction and electrorheological fluid switches for tuned vibration absorbers, J. Sound. Vib. 460 (2019) 114874. doi:10.1016/j.jsv.2019.114874.

[6] S.-B. Choi, Y.-M. Han, Vibration control of electrorheological seat suspension with human-body model using sliding mode control, J. Sound. Vib. 303 (2007) 391–404. doi:10.1016/j.jsv.2007.01.027.

[7] J. N. Potter, S. A. Neild, D. J. Wagg, Quasi-active suspension design using magnetorheological dampers, J. Sound. Vib. 330 (2011) 2201–2219. doi:10.1016/j.jsv.2010.11.029.

[8] X. B. Nguyen, T. Komatsuzaki, Y. Iwata, H. Asanuma, Robust adaptive controller for semi-active control of uncertain structures using a magnetorheological elastomer-based isolator, J. Sound. Vib. 434 (2018) 192–212. doi:10.1016/j.jsv.2018.07.047.

[9] A. Rossi, F. Orsini, A. Scorza, F. Botta, N. P. Belfiore, S. A. Sciuto, A review on parametric dynamic models of magnetorheological dampers and their characterization methods, Actuators 7 (2) (2018) 16. doi:10.3390/act7020016.

[10] B. Kim, J.-y. Yoon, Enhanced adaptive filtering algorithm based on sliding mode control for active vibration rejection of smart beam structures, Appl. Sci. 7 (7) (2017) 750. doi:10.3390/app7070750.

[11] L. Pernod, B. Lossouarn, J.-A. Astolfi, J.-F. Deü, Vibration damping of marine lifting surfaces with resonant piezoelectric shunts, J. Sound. Vib. 496 (2021) 115921. doi:10.1016/j.jsv.2020.115921.

[12] H. He, X. Tan, J. He, F. Zhang, G. Chen, A novel ring-shaped vibration damper based on piezoelectric shunt damping: Theoretical analysis and experiments, J. Sound. Vib. 468 (2020) 115125. doi:10.1016/j.jsv.2019.115125.

[13] R. Darleux, B. Lossouarn, J.-F. Deü, Passive self-tuning inductor for piezoelectric shunt damping considering temperature variations, J. Sound. Vib. 432 (2018) 105–118. doi:10.1016/j.jsv.2018.06.017.

[14] M. Pohl, M. Rose, Piezoelectric shunt damping of a circular saw blade with autonomous power supply for noise and vibration reduction, J. Sound. Vib. 361 (2016) 20–31. doi:10.1016/j.jsv.2015.09.021.

[15] A. Erturk, D. J. Inman, On mechanical modeling of cantilevered piezoelectric vibration energy harvesters, J. Intel. Mat. Syst. Str. 19 (11) (2008) 1311–1325. doi:10.1177/1045389X07085639.

[16] M. Rezaei, R. Talebitooti, S. Rahmanian, Efficient energy harvesting from nonlinear vibrations of pzt beam under simultaneous resonances, Energy 182 (2019) 369–380. doi:10.1016/j.energy.2019.05.212.

[17] L. Yu, L. Tang, T. Yang, Piezoelectric passive self-tuning energy harvester based on a beam-slider structure, J. Sound. Vib. 489 (2020) 115689. doi:10.1016/j.jsv.2020.115689.

[18] D. W. Dareing, T. Thundat, S. Jeon, M. Nicholson, Modal analysis of microcantilever sensors with environmental damping, J. Appl. Phys. 97 (2005) 084902. doi:10.1063/1.1880472.

[19] F. Botta, A. Rossi, N. P. Belfiore, A feasibility study of a novel piezo mems tweezer for soft materials characterization, Appl. Sci. 9 (2019) 2277. doi:10.3390/app9112277.

[20] S. Naduvinamani, N. C. Iyer, Design and simulation of pzt based MEMS piezoelectric accelerometer, in: Proc. and Optimization Techniques (ICEEOT), Chennai, India, 2016,, 2016, pp. 3715–3721.

[21] G. Li, Z. Yi, Y. Hu, J. Liu, B. Yang, High-performance low-frequency mems energy harvester via partially covering pzt thick film, J. Micromech. Microeng. 28 (9) (2018) 095007. doi:10.1088/1361-6439/aac58a.

[22] P. Belardinelli, S. N. F. D. Souza, E. Verlinden, J. Wei, U. Staufer, F. Alijani, M. K. Ghatkesar, Second flexural and torsional modes of vibration in suspended microfluidic resonator for liquid density measurements, J. Micromech. Microeng. 30 (2020) 055003. doi:10.1088/1361-6439/ab772c.

[23] L. Gonzalez, M. Rodrigues, A. M. Benito, L. Pérez-García, M. Puig-Vidal, J. Otero, Piezoelectric tuning fork biosensors for the quantitative measurement of biomolecular interactions, Nanotechnology 26 (2015) 495502. doi:10.1088/0957-4484/26/49/495502.

[24] C.-Y. Lee, J.-H. Lin, Incorporating piezoelectric energy harvester in tunable vibration absorber for application in multi-modal vibration reduction of a platform structure, J. Sound. Vib. 389 (2017) 73–88. doi:10.1016/j.jsv.2016.11.007.

[25] G. Ferrari, M. Amabili, Active vibration control of a sandwich plate by non-collocated positive position feedback, J. Sound. Vib. 342 (2015) 44–56. doi:10.1016/j.jsv.2014.12.019.

[26] A. Loghmani, M. Danesh, M. K. Kwak, M. Keshmiri, Vibration suppression of a piezo-equipped cylindrical shell in a broad-band frequency domain, J. Sound. Vib. 411 (2017) 260–277. doi:10.1016/j.jsv.2017.08.051.

[27] K. Bendine, F. B. Boukhoulda, B. Haddag, M. Nouari, Active vibration control of composite plate with optimal placement of piezoelectric patches, Mech. Adv. Mater. Struct. 26 (4) (2019) 341–349. doi:10.1080/15376494.2017.1387324.

[28] J. Qiu, H. Ji, K. Zhu, Semi-active vibration control using piezoelectric actuators in smart structures, Front. Mech. Eng. 4 (3) (2009) 242–251. doi:10.1007/s11465-009-0068-z.

[29] M. I. Frecker, Recent advances in optimization of smart structures and actuators, J. Intel. Mat. Syst. Str. 14 (4-5) (2003) 207–216. doi:10.1177/1045389X03031062.

[30] V. Gupta, M. Sharma, N. Thakur, Optimization criteria for optimal placement of piezoelectric sensors and actuators on a smart structure: a technical review, J. Intel. Mat. Syst. Str. 21 (12) (2010) 1227–1243. doi:10.1177/1045389X10381659.

[31] E. F. Crawley, J. De Luis, Use of piezoelectric actuators as elements of intelligent structures, AIAA J 25 (10) (1987) 1373–1385. doi:10.2514/3.9792.

[32] K. Dhuri, P. Seshu, Piezo actuator placement and sizing for good control effectiveness and minimal change in original system dynamics, Smart Mater. Struct. 15 (6) (2006) 1661. doi:10.1088/0964-1726/15/6/019.

[33] K. R. Kumar, S. Narayanan, Active vibration control of beams with optimal placement of piezoelectric sensor/actuator pairs, Smart Mater. Struct. 17 (5) (2008) 055008. doi:10.1088/0964-1726/17/5/055008.

[34] M. A. Demetriou, A numerical algorithm for the optimal placement of actuators and sensors for flexible structures, in: Proceedings of the 2000 American Control Conference. ACC (IEEE Cat. No.00CH36334), Chicago, IL, USA, 2000, Vol. 4, 2000, pp. 2290–2294 vol.4. doi:10.1109/ACC.2000.878588.

[35] I. Bruant, G. Coffignal, F. Lene, M. Verge, A methodology for determination of piezoelectric actuator and sensor location on beam structures, J. Sound. Vib. 243 (5) (2001) 861–882. doi:10.1006/jsvi.2000.3448.

[36] M. Sunar, S. Rao, Distributed modeling and actuator location for piezoelectric control systems, AIAA J. 34 (10) (1996) 2209–2211. doi:10.2514/3.13380.

[37] Y. Yang, Z. Jin, C. K. Soh, Integrated optimal design of vibration control system for smart beams using genetic algorithms, J. Sound. Vib. 282 (3-5) (2005) 1293–1307. doi:10.1016/j.jsv.2004.03.048.

[38] R. Barboni, A. Mannini, E. Fantini, P. Gaudenzi, Optimal placement of pzt actuators for the control of beam dynamics, Smart Mater. Struct. 9 (1) (2000) 110. doi:10.1088/0964-1726/9/1/312.

[39] Q. Wang, C. M. Wang, Optimal placement and size of piezoelectric patches on beams from the controllability perspective, Smart Mater. Struct. 9 (4) (2000) 558. doi:10.1088/0964-1726/9/4/320.

[40] A. Hohl, M. Neubauer, S. M. Schwarzendahl, L. Panning, J. Wallaschek, Active and semiactive vibration damping of turbine blades with piezoceramics, in: Active and Passive Smart Structures and Integrated Systems, vol.7288 of Proceedings of SPIE, San Diego, California, USA, March, 2009. doi:10.1117/12.815800.

[41] A. J. Provenza, C. R. Morrison, Control of fan blade vibrations using piezoelectrics and bi-directional telemetry, in: Proceedings of the ASME Turbo Expo, Vancouver, Canada, June, 2011. doi:10.1115/gt2011-46714.

[42] X. Wang, W. Zhou, Z. Wu, W. Wu, Optimal unimorph and bimorph configurations of piezocomposite actuators for bending and twisting vibration control of plate structures, J. Intel. Mat. Syst. Str. 29 (8) (2018) 1685–1696. doi:10.1177/1045389x17742736.

[43] L. Wang, V. Hofmann, F. Bai, J. Jin, J. Twiefel, Modeling of coupled longitudinal and bending vibrations in a sandwich type piezoelectric transducer utilizing the transfer matrix method, Mech. Syst. Signal Pr. 108 (2018) 216–237. doi:10.1016/j.ymssp.2018.02.022.

[44] F. Botta, N. Marx, S. Gentili, C. Schwingshackl, L. Di Mare, G. Cerri, D. Dini, Optimal placement of piezoelectric plates for active vibration control of gas turbine blades: experimental results, in: Sensors and Smart

Structures Technologies for Civil, Mechanical, and Aerospace Systems, Vol. 8345 of SPIE Smart Structures and Materials + Nondestructive Evaluation and Health Monitoring, 2012, San Diego, California, United States, 2012, pp. 180–184. doi:10.1117/12.915266.

[45] F. Botta, D. Dini, C. Schwingshackl, L. di Mare, G. Cerri, Optimal placement of piezoelectric plates to control multimode vibrations of a beam, Adv. in Acoust. and Vib. 2013 (2013) 1–8, art. no. 905160. doi:10.1155/2013/905160.

[46] F. Botta, A. Rossi, L. Schinaia, A. Scorza, F. Orsini, S. Sciuto, N. Belfiore, Experimental validation on optimal placement of pzt plates for active beam multimode vibrations reduction, in: AIMETA 2017 Proceedings of the 23rd Conference of the Italian Association of Theoretical and Applied Mechanics, Salerno (Italy), 4-7 Settembre, Vol. 3, 2017, pp. 2258–2269.

[47] F. Botta, A. Scorza, A. Rossi, Optimal piezoelectric potential distribution for controlling multimode vibrations, Appl. Sci. 8 (4) (2018) 551. doi:10.3390/app8040551.

[48] K. R. V. Kaza, R. E. Kielb, Effects of warping and pretwist on torsional vibration of rotating beams, J. Appl. Mech. 51 (1984) 913–920. doi:10.1115/1.3167746.

[49] T. R. Kane, R. R. Ryan, A. K. Banerjeer, Dynamics of a cantilever beam attached to a moving base, J. Guid. Control Dynam. 10 (2) (1987) 139–151. doi:10.2514/3.20195.

[50] J. S. Rao, Turbomachine blade vibration, Wiley, New York, N.Y., 1991.

[51] J. S. Rao, Turbine blade life estimation, Alpha Science International Ltd (India), 2000.

[52] H. P. Lee, Dynamic stability of a rotating cantilever beam with in-plane base acceleration, Eng. Computation 14 (1997) 471–480. doi:10.1108/02644409710178520.

[53] Y.-J. Chiu, D.-Z. Chen, The coupled vibration in a rotating multi-disk rotor system, Int. J. Mech. Sci. 53 (2011) 1–10. doi:10.1016/j.ijmecsci.2010.10.001.

[54] P. Łabedzki, R. Pawlikowski, A. Radowicz, Transverse vibration of a cantilever beam under base excitation using fractional rheological model, in: AIP Conf. Proc., Vol. 2029, AIP Publishing LLC, 2018, p. 020034. doi:10.1063/1.5066496.

[55] F. Wang, A. Abedini, T. Alghamdi, S. Onsorynezhad, Bimodal approach of a frequency-up-conversion piezoelectric energy harvester, Int. J. Struct. Stab. Dyn. 19 (2019) 1950090. doi:10.1142/s0219455419500901.

[56] C. E. Repetto, A. Roatta, R. J. Welti, Forced vibrations of a cantilever beam, Eur. J. Phys. 33 (5) (2012) 1187–1195. doi:10.1088/0143-0807/33/5/1187.

[57] N. Jalili, M. Dadfarnia, F. Hong, S. S. Ge, Adaptive non model-based piezoelectric control of flexible beams with translational base, in: Proceedings of the American Control Conference, Anchorage, AK May 8-1 0, 2002, 2002. doi:10.1109/acc.2002.1024520.

[58] A. Preumont, Vibration control of active structures: an introduction., Springer Netherlands, 2011. doi:10.1007/978-94-007-2033-6.

[59] M. E. Alam, J. L. Kauffman, A. K. Dickerson, Drop ejection from vibrating damped, dampened wings, Soft Matter 16 (2020) 1931–1940. doi:10.1039/c9sm02253h.

[60] S. El-Borgi, R. Fernandes, P. Rajendran, R. Yazbeck, J. G. Boyd, D. C. Lagoudas, Multiple bandgap formation in a locally resonant linear metamaterial beam: Theory and experiments, J. Sound. Vib. 488 (2020) 115647. doi:10.1016/j.jsv.2020.115647.

[61] J. M. Kluger, T. P. Sapsis, A. H. Slocum, Robust energy harvesting from walking vibrations by means of nonlinear cantilever beams, J. Sound. Vib. 341 (2015) 174–194. doi:10.1016/j.jsv.2014.11.035.

[62] R.-F. Fung, Y.-T. Liu, C.-C. Wang, Dynamic model of an electromagnetic actuator for vibration control of a cantilever beam with a tip mass, J. Sound. Vib. 288 (2005) 957–980. doi:10.1016/j.jsv.2005.01.046.

[63] L. Schinaia, A. Scorza, F. Botta, A. Rossi, R. Maiozzi, F. Orsini, S. A. Sciuto, A novel, low-cost and reliable workbench for optimal voltage distribution on piezoelectric array actuators, Actuators 8 (1) (2019) 6. doi:10.3390/act8010006.

[64] E. K. Armstrong, R. E. Stevenson, Some practical aspects of compressor blade vibration, The Aeronautical Journal 64 (591) (1960) 117–130. doi:10.1017/s0368393100072242.

[65] J. Gallego-Garrido, G. Dimitriadis, J. R. Wright, A class of methods for the analysis of blade tip timing data from bladed assemblies undergoing simultaneous resonances - part i: theoretical development, Int. J. Rotating Mach. 2007. doi:10.1155/2007/27247.

[66] J. Gallego-Garrido, G. Dimitriadis, I. B. Carrington, J. R. Wright, A class of methods for the analysis of blade tip timing data from bladed assemblies undergoing simultaneous resonances - part ii: experimental validation, Int. J. Rotating Mach. 2007 (2007) 1–10. doi:10.1155/2007/73624.